



HAL
open science

Pockmarks on the South Aquitaine Margin continental slope: the seabed expression of past fluid circulation and bottom currents

Guillaume Michel, Stéphanie Dupré, Agnès Baltzer, Axel Ehrhold, Patrice Imbert, Mathilde Pitel, Benoît Loubrieu, Carla Scalabrin, Pascal Lazure, Louis Marié, et al.

► To cite this version:

Guillaume Michel, Stéphanie Dupré, Agnès Baltzer, Axel Ehrhold, Patrice Imbert, et al.. Pockmarks on the South Aquitaine Margin continental slope: the seabed expression of past fluid circulation and bottom currents. *Comptes Rendus Géoscience*, 2017, 349 (8), pp.391 - 401. 10.1016/j.crte.2017.10.003 . hal-01704712

HAL Id: hal-01704712

<https://ifp.hal.science/hal-01704712v2>

Submitted on 15 Sep 2020

HAL is a multi-disciplinary open access archive for the deposit and dissemination of scientific research documents, whether they are published or not. The documents may come from teaching and research institutions in France or abroad, or from public or private research centers.

L'archive ouverte pluridisciplinaire **HAL**, est destinée au dépôt et à la diffusion de documents scientifiques de niveau recherche, publiés ou non, émanant des établissements d'enseignement et de recherche français ou étrangers, des laboratoires publics ou privés.

1 Pockmarks on the South Aquitaine Margin continental slope: the
2 seabed expression of past fluid circulation and former bottom currents

3 **Authors**

4 Michel G. (1), Dupré S. (1), Baltzer A. (2), Ehrhold A. (1), Imbert P. (3), Pitel M. (1), Loubrieu B. (1),
5 Scalabrin C. (1), Pascal Lazure, Louis Marié, Geldof J.B. (4), Deville E. (5).

6 (1) IFREMER – Unité Géosciences Marines, 29280 Plouzané, France

7 (2) Université de Nantes, CNRS, UMR6554 – 44312 Nantes Cedex 3, France

8 (3) TOTAL – Centre Scientifique et Technique Jean Féger. Avenue Larribau, 64018 Pau Cedex, France

9 (4) TOTAL –10 Place des Vosges, 92072 Paris La Défense, France

10 (5) IFPEN –1 et 4 avenue de Bois Préau - 92852 Rueil-Malmaison, France

11

12 **Corresponding Author**

13 Guillaume MICHEL

14 Tel: +33 6 79 75 08 27

15 E-mail address: guillaume.michel@ifremer.fr

16 **Abstract**

17 Inactive and mostly elongated pockmarks of 100-200 m in dimension were recently
18 discovered on the South Aquitaine Margin continental slope. They are distributed at water
19 depths greater than 350 m in both interfluvial and sediment wave areas, and are strongly
20 controlled by the sedimentary morphology and architecture. Water column and seafloor
21 backscatter and sub-bottom profiler data do not exhibit present-day or past gas evidence, e. g.
22 massive and continuous gas releases at the seabed and fossil methane-derived authigenic
23 carbonates. It is thus proposed that the pockmarks originated from a shallow source and result
24 from relatively recent and short-duration gas or water expulsion events. Former near-bottom
25 currents may have contributed to the elongation of these WNW-ESE oriented pockmarks

26 whereas present-day weaker near-bottom currents may induce upwelling, contributing to the
27 maintenance of the elongated shapes of the pockmarks.

28 **Keywords**

29 Pockmark, fluid, seabed morphology, Aquitaine slope, GIS, currents

30 **1. Introduction**

31 Pockmarks were first described by King and MacLean (1970) as seafloor morphological
32 depressions, formed by fluid escapes. Pockmarks are commonly encountered and, are
33 worldwide, related to fluid migrating upward (Judd and Hovland, 2007) and triggering-
34 sediment resuspension during leakage and sediment collapse. These depressions are observed
35 from shallow environments (Rise et al., 2015) to deep bathyal environments (Gay et al.,
36 2006). Pockmark morphologies can be associated with various types of fluids and processes,
37 e. g. small scale pockmarks can be related to a unique local gas source (Gay et al., 2007), to
38 dewatering of the sediments upon compaction (Harrington, 1985) and to freshwater seeps
39 (Whiticar, 2002) while pluri-kilometre-scale pockmarks may indicate hydrate dissolution
40 (Sultan et al., 2010). Pockmarks may occur as clusters (Hovland et al., 2010) or as strings of
41 pockmarks (Pilcher and Argent, 2007). Strings of pockmarks are commonly related to
42 geological features focusing fluid flows, e. g. fractures and faults (Gay et al., 2007) and buried
43 valleys (Baltzer et al., 2014).

44 The modification of original pockmark morphologies will depend on internal factors such
45 as successive fluid expulsion events (Judd and Hovland, 2007), the presence of methane-
46 derived authigenic carbonates (Gay et al., 2006) and external factors such as bottom currents
47 (Bøe et al., 1998; Josenhans et al., 1978; Schattner et al., 2016), slumping and sedimentary
48 destabilization along the slope direction (Brothers et al., 2014), presence of benthic fauna and

49 debris accumulation (Webb et al., 2009), e. g. coarser sediments (Pau and Hammer, 2013).
50 Bottom currents may contribute to elongate pockmarks along the direction of the currents by
51 eroding sediments and preventing sedimentation over the pockmarks (Andresen et al., 2008;
52 Dandapath et al., 2010). Bottom currents may induce upwelling within the pockmarks that
53 would limit the sedimentation of fine-grained sediments, therefore maintaining pockmark
54 morphology (Brothers et al., 2011; Hammer et al., 2009; Pau et al., 2014). Moreover,
55 coalescent pockmarks (merging depressions) (Gay et al., 2006) may be a result of successive
56 fluid escapes or external processes as cited above, eventually forming elongated pockmarks.
57 Pockmark morphological characteristics, accessible through their acoustic signature, may be
58 used to determine potential activity (Dupré et al., 2010; Hovland et al., 2010), and the nature
59 of fluids involved (Gay et al., 2006; Judd and Hovland, 2007) and also to address the relative
60 timing of pockmark formation with regards to surrounding sedimentation (Bayon et al., 2009).
61 The present study mainly focuses on the geophysical characterization of a wide pockmark
62 field discovered on the continental slope of the Aquitaine Margin (offshore France) in 2013
63 during the GAZCOGNE1 oceanographic expedition. Pockmark activity and the nature of
64 fluids involved in pockmark formation are discussed. Particular attention is paid to the
65 pockmark reshaping related to external factors such as bottom currents.

66 **2. The setting**

67 Related to the opening of the North Atlantic Ocean, the Bay of Biscay initially
68 corresponded to a V-shaped rift, initiated during the Late Jurassic and aborted in the mid-
69 Upper Cretaceous (Roca et al., 2011). Its extensional phase was stopped during the Santonian
70 age by the opening of the South Atlantic Ocean. The subsequent northward drift of the Iberian
71 plate and the related compression phase led to Pyrenean orogeny (Roca et al., 2011). The Bay
72 of Biscay is surrounded by different shelves, the large Armorican Shelf, the Aquitaine Shelf,

73 the Basque Shelf and the Iberian Shelf (Fig. 1) with a major morphological high, the Landes
74 Plateau. The hydrocarbon Parentis Basin, created during the Pyrenean Orogeny, extends from
75 the onshore to the offshore domain, in the south part of the Aquitaine Shelf (Biteau et al.,
76 2006) (Fig. 1).

77 **FIG 1**

78 The study area is located in the French EEZ (Exclusive Economic Zone) on the
79 continental slope of the Aquitaine Shelf, from 200 m to 1600 m water depths, with a mean
80 smooth slope of $\sim 3^\circ$ (Figs 1 and 2). This area is 60-80 km westward of the coastline, between
81 the Cap Ferret Canyon ($44^\circ 40'$ N) and the Capbreton Canyon ($43^\circ 30'$ N). The study area can
82 be divided into two main morphological domains. The northern part, from $44^\circ 35' 50''$ N to
83 $44^\circ 11' 44''$ N latitude, is deeply incised by E-W oriented canyons with heads rooted at the
84 shelf break edge. There, the inter-canyon areas are kilometre wide along the N-S axis (Fig.
85 2a) and are affected by slope instabilities within a context of silt dominated sedimentation
86 (Schmidt et al., 2014). The southern part, from $44^\circ 11' 44''$ N to $43^\circ 52' 37''$ N latitude, does not
87 show any canyons, only some landslide scarps located at 230 m water depth and a wide
88 sediment wave field located between 250 and 1000 m water depth (Fig. 2), with a surficial
89 sandy silt sedimentation, extending from the shelf break to the foot slope (Faugères et al.,
90 2002; Gonthier et al., 2006). Sediment wave morphologies, with wave lengths between 800 m
91 and 1600 m and heights from 20 m to 70 m show crests slightly oriented at an oblique angle
92 of the main slope, between 010° N and 035° N. The influence of bottom currents in the
93 formation processes of sedimentary waves along the Aquitaine slope has been indicated
94 (Faugères et al., 2002; Gonthier et al., 2006). The sedimentary waves are covered by a thin
95 homogenous layer corresponding to the U4 unit described by Faugères et al. (2002), which is
96 12-15 metres thick (Gonthier et al., 2006) and pinches out on the upper slope between 400
97 and 300 m water depth. The surficial sedimentary cover of the Aquitaine Shelf is mainly

98 composed of sand and silty sand (Cirac et al., 2000). Inactive pockforms and pockmarks have
99 been described on the Landes Plateau (Baudon et al., 2013; Iglesias et al., 2010) and on the
100 Basque Shelf (Gillet et al., 2008), respectively. Recently, Dupré et al. (2014) described an
101 active cold seep system at the edge of the Aquitaine shelf without any pockmarks.

102 The hydrography regime of the study area appears to be complex due to the semi-
103 enclosed morphology of the Bay of Biscay and the interaction between different currents of
104 different time scales, meso-tidal currents (Batifoulier et al., 2012; Charria et al., 2013; Le
105 Boyer et al., 2013), contour currents (Van Aken, 2000) and some temporary currents related
106 to wind-forced events (Kersalé et al., 2016).

107 **3. Data and methods**

108 **3.1. Geophysical data acquisition and processing**

109 High-resolution marine geophysical data were acquired during the BOBGEO2
110 expedition in 2010 and more significantly during the GAZCOGNE1 survey in 2013 covering
111 3200 km² of the seafloor at water depths ranging from 130 m to 1600 m (Fig. 2). During the
112 GAZCOGNE1 survey, multibeam bathymetry, water column and seafloor backscatter and
113 seismic reflection (sub-bottom profiler) data were acquired simultaneously. Multibeam data
114 were collected onboard the R/V Le Suroît with a Kongsberg EM302 ship-borne multibeam
115 echosounder operated at a frequency of 30 kHz with the celerity profile calibrated with
116 ©Sippican shots. Seafloor multibeam data were processed through CARAIBES software
117 (©IFREMER) with application of bathymetric filters and correction of position, pitch, roll
118 and tide effects for raw bathymetric data and with the generation of a compensation curve to
119 harmonize values along the survey lines for seafloor backscatter data. Both bathymetry and
120 seafloor backscatter processed data were mainly exported to mosaic grids of 15x15 m (with
121 some backscatter maps at 10x10 m cells). Water column backscatter data only recorded

122 during the GAZCOGNE1 marine expedition were processed in SonarScope software
123 (©IFREMER) and then interpreted in GLOBE/3DViewer (©IFREMER) (Dupré et al., 2015).

124 The sub-bottom profiles were recorded with the ship-borne sub-bottom profiler
125 ECHOES 3500 ©T7iXblue emitting a linear frequency modulated signal, ranging from 1.8 to
126 5.3 kHz, with a vertical resolution of 10 cm and a maximum vertical penetration of 100 m. A
127 2D sub-bottom profiler insonifies a surface at the seafloor defined by the Fresnel equation and
128 may record lateral reflexions from close-by 3D features, as well as artefacts. These artefacts
129 may be displayed as diffraction hyperbola (Dupré et al., 2014b) and triplication points, so-
130 called "bow ties" (Moss et al., 2012). Raw data were processed with QC-SUBOP software
131 (©IFREMER) before being exported in SEG-Y and then interpreted in ©Kingdom software
132 (Fig. 3). The water current data were acquired during the ASPEX2010A mooring survey (Le
133 Boyer et al., 2013) with an Acoustic Doppler Current Profiler (ADCP) operated at a
134 frequency of 75 kHz and recording every 2 minutes. The data discussed in this paper come
135 from mooring 10 located at 44°00.069'N - 02°08.644'W at 450 m water depth in the sediment
136 wave field (Figs. 2a and c). Water current data were recorded over more than 6 months (18th
137 July 2009 - 30th January 2010). Current velocities were integrated between 17 m and 33 m
138 above the seafloor and averaged every 20 minutes. Classic harmonic tide analyses were
139 conducted on ASPEX current data to extract tide-related signals from the raw signal (Lazure
140 et al., 2009).

141 **3.2. Pockmark morphometry**

142 All pockmarks were manually delimited, identified by their rim on the slope grid
143 (processed at 15 m and calculated with Slope function in Spatial Analyst toolbox from
144 Arcmap 10.2, ©ESRI). It is worth noting that below the bathymetry resolution (15 m),
145 detection cannot be performed effectively. In other words, small pockmarks of diameter
146 <30 m, if present, could not have been mapped.

147 Eleven morphological attributes were extracted from GIS for each pockmark: its area,
148 perimeter, area/perimeter ratio, internal depth (from the rim down to the apex of the
149 pockmark), minor and major axis lengths, major axis direction, elongation (major/minor axis
150 length ratio), bathymetry, slope within the pockmark and morphological domain. The
151 morphological attributes of the Aquitaine slope pockmarks are available online as a SEANOE
152 public database with information on pockmark location and seafloor backscatter data (Michel
153 et al., 2017).

154 FIG 2

155 4. Results

156 4.1. Pockmark spatial distribution

157 606 pockmarks were discovered, exclusively located on the continental slope, from
158 350 m water depth in the upper slope down to 1150 m water depth, covering 800 km² (Fig. 2).
159 The oceanward extension of the pockmarks is limited by the survey acquisition (Fig. 2). The
160 mapped pockmarks are relatively large, with regards to known pockmarks (Judd and Hovland,
161 2007; Pilcher and Argent, 2007), with a rough diameter from 52 to 330 m and an internal
162 depth up to 42 m for the largest pockmarks (Fig. 4a). The majority of the pockmarks (80%)
163 have a rough diameter between 100 and 200 m for an average internal depth of 15 m
164 (Appendix B).

165 72% (434 units) of the pockmarks occur in the inter-canyon areas (574 km²) and 25%
166 (153 units) in the sediment wave field (374 km²) (Figs. 2 and 5). Pockmark density in the
167 inter-canyon domain is twice as high as in the sediment wave field. The 3% (19 units)
168 remaining pockmarks are located deeper at the foot slope (Fig. 2). In the northern part of the
169 studied area, the pockmarks are completely absent from the canyons. Confined within the
170 inter-canyons, the pockmarks spread along an E-W direction. The pockmarks are distributed

171 both at the summits of the antiforms (see e. g. the second northern inter-canyon in Fig. 2) and
172 at the borders of the canyons (see e. g. the southern border of the inter-canyon at 44°17'N in
173 Fig. 2). The majority of the pockmarks do not form alignments or so called pockmark trains.
174 Their distribution is more diffuse within each inter-canyon area unless the inter-canyons are
175 narrow (see e. g. the inter-canyon at 44°13'N in Fig. 2). A few pockmark clusters are also
176 observed (Fig. 2) with densities up to 12 pockmarks per km². Locally, a few coalescent
177 pockmarks appear to form elongated pockmarks (Fig. 2b). In the sediment wave field,
178 pockmarks are located both on the wave crests (36%) and between the crests (48%), as
179 noticed by Baudon et al. (2013) for similar pockmarks located on the upper slope of the
180 Aquitaine slope south of the studied area. The 16% remaining pockmarks are located on
181 relatively flat areas without any spatial organisation. Therefore, the main regional pockmark
182 repartition in the sediment wave domain follows the sediment wave's crests and inter-crests
183 direction between N010 and N035 (Figs 2a, c) rather than an E-W direction. Locally, a few
184 pockmark strings (maximum 8 depressions along 2 km), only concerning less than 13% of the
185 153 pockmarks mapped in the sediment wave field, are observed related to sediment wave
186 orientation (Figs 2a and c). From the northern part of the sediment wave field to the southern
187 part, the pockmark density increases and pockmarks are also located deeper in the slope.
188 Pockmarks are however absent from two main corridors crossing the sediment wave field
189 with a convergence and narrowing of the pockmark field downslope (see uppermost part of
190 Fig. 2c).

191 **4.2. Pockmark characterization**

192 **4.2.1. Acoustic signature of water column and surficial sediments**

193 The EM302 water column backscatter data from the GAZCOGNE1 marine expedition
194 do not exhibit any amplitude anomaly in the water column related to gas bubble escapes, and

195 this throughout the pockmark field and over the 6 days of the acoustic survey (28th July to 2nd
196 August 2013).

197 The average seafloor backscatter amplitude within the pockmarks (excluding 57
198 pockmarks located at the vertical of the ship track where the data are worthless) ranges from -
199 34.5 to -21.8 dB in the inter-canyons with a mean value of -27.2 dB (Fig. 4b). The seafloor
200 backscatter amplitude values vary from -31.6 to -22.6 dB with a mean value of -27.1 dB in the
201 sediment wave field (Fig. 4b). The seafloor backscatter of surrounding sediment, calculated
202 within a 100 m buffer around the pockmark rim, vary from -34 dB to -23 dB with a mean
203 value of -27 dB. The EM302 seafloor backscatter values in the majority of the pockmarks are
204 similar to the ones of surficial sediments around wherever pockmarks are located in inter-
205 canyon or sediment wave field domains. Only a small percentage of the pockmarks exhibits,
206 within part of the depression, high or low seafloor backscatter amplitudes that contrast with
207 the surrounding seafloor.

208 **4.2.2. Seismic investigation at the seabed and inside the sediment pile**

209 The acquired sub-bottom profiler lines only cross 38 pockmarks. The profiles do not
210 exhibit any high seafloor amplitude anomalies, e. g. enhanced reflectors, or high amplitude
211 anomalies within the uppermost 100 m of sediment (Fig. 3). Only triplication points due to
212 geometry artefacts below pockmarks are observed. The sedimentary records below and
213 besides the pockmarks are not disturbed. Moreover, no distinct draped sediment layers are
214 observed within the depressions with regards to the ten centimetres resolution from the sub-
215 bottom profiler.

216 **FIG 3**

217 **4.2.3. Pockmark morphometry**

218

219 The pockmark surface ranges from $0.29 \times 10^4 \text{ m}^2$ to $7.49 \times 10^4 \text{ m}^2$ at the inter-canyon
220 area and from $0.25 \times 10^4 \text{ m}^2$ to $6 \times 10^4 \text{ m}^2$ in the sediment wave field area. The mean value of
221 pockmark surface is $1.8 \times 10^4 \text{ m}^2$ in the inter-canyon and $1.7 \times 10^4 \text{ m}^2$ in the sediment wave field
222 (Fig. 4a). The variations in pockmark size are similar in both morphological domains. A
223 general increase in pockmark surface is observed at shallower water depths but no linear trend
224 is observed (regression line, $R^2= 0.1259$ in the inter-canyon area and $R^2=0.1895$ in the
225 sediment wave field) (Appendix B).

226 **FIG 4**

227 The pockmark internal depth ranges from 4 to 42 m with a mean value of 15 m
228 (Appendix B). The deepest internal depth values correspond to the largest pockmarks
229 (>200 m in diameter) with a mean value of 22 m.

230 The pockmark elongation ranges from 1 to 5.7 with a mean value of 1.4 on the inter-
231 canyon area and from 1 to 2.7 with a mean value of 1.4 in the sediment wave field (Fig. 4c).
232 Most of the pockmarks (88%) are elongated with an elongation superior to 1.1 while only
233 12% are sub-circular (elongation between 1 and 1.1) (Fig. 2). Elongation values <1.1 are
234 considered as sub-circular shapes in order to take into account potential mapping biases and
235 calculation approximation. Among the elongated pockmarks, a majority have an elongation
236 between 1.1 and 1.5 (66%) while 19% have an elongation between 1.5 and 2.2. The most
237 elongated pockmarks with an elongation >2.2 are less common (3%) and mainly correspond
238 to coalescent pockmarks (Fig. 2b, most south-eastern pockmarks).

239 The major axis direction of the pockmarks with elongation values >1.5 (134 units) has
240 been compared to the surrounding slope value (Fig. 5). These pockmarks correspond to 92
241 depressions in the inter-canyon domain and 42 in the sediment wave field. In the inter-canyon
242 domain, local slope orientation around the pockmarks is mostly E-W while the pockmark
243 major axis is mostly NW-SE, with 40% of them oriented N150-330 and 35% others oriented

244 N120-300. In the sediment wave field, the local slope around the pockmarks is oriented
245 around N300 and the pockmark major axes are mostly oriented WNW-ESE, 40% of them
246 oriented N100-280 and 22% oriented N120-300.

247 **FIG 5**

248 **4.3. Bottom currents in the sediment wave field**

249 Current direction and amplitude distributions are displayed in current roses (Fig. 5) with
250 E-W and N-S current components (Appendix C). Current velocities derived from the raw
251 signal are mostly lower than 10 cm/s (90% of the records for the E-W component and 81% for
252 the N-S component) (Fig. 5c) with the maximum amplitude reaching 34 cm/s during two
253 events, 10 days apart, over the 6 months of the acquisition. Currents vary on different time
254 scales, associated with different forcing factors. A large-amplitude semi-diurnal tidal signal
255 (current vector period close to 12 hours, current amplitude period close to 6 hours) coexists
256 with weaker signals that have longer periods (approximately one week). The tidal signal is
257 mostly oriented E-W, and exhibits a significant cross-slope component. The longer-period
258 component (red curves in Appendix C) is oriented along-slope due to the geostrophic
259 constraint, as evidenced by the red dots in Fig. 5. Its cross-slope component is always smaller
260 than 5 cm/s. The along-slope component is almost always weaker than the tidal current (for
261 81 % of the records), but can reach high instantaneous values during specific events (higher
262 than 15 cm/s, 6% of occurrence).

263 **5. Discussion**

264 **5.1. Pockmark inactivity and nature of the fluids involved**

265 Free gas leakage produces clear water column backscatter anomalies commonly used
266 to attest seepage activity (Dupré et al., 2015). During the GAZCOGNE1 survey, no water

267 column acoustic anomalies corresponding to gas bubbles were detected in the whole slope
268 area. Although the temporal variability of seepage activity may be invoked, the 6 days of the
269 acoustic survey are sufficient to cover the time window for the tidal cycle which could be a
270 possible triggering mechanism (Baltzer et al., 2014). Thus, pockmarks along the Aquitaine
271 slope are interpreted as currently inactive in terms of free gas seepage.

272 Considering the sediment cover, methane-derived authigenic carbonates are
273 considered as confident indicators of long-term gas circulation (Bayon et al., 2009). Outcrops
274 and sub-outcrops of carbonate structures are easily detected on seafloor backscatter data as
275 occurrence of high amplitude anomaly patches (Dupré et al., 2010). The lack of high seafloor
276 backscatter values within the pockmarks and the similarity of seafloor acoustic signature
277 between the pockmarks and the surrounding sediments clearly provide evidence for the
278 absence of methane-derived authigenic carbonates along the Aquitaine slope.

279 Within the uppermost 100 m of the sediment, sub-bottom profiles across pockmarks
280 do not exhibit any enhanced reflectors and diffracting points at the seabed pile that carbonates
281 would seismically produce if present (Dupré et al., 2010). No acoustic blanking, blank
282 chimneys or any other seismic evidence of gas accumulations within the vertical resolution
283 limit of twenty centimetres are observed. At the present day, the absence of acoustic
284 anomalies within sedimentary records excludes the occurrence of 1) layers charged with free
285 gas, 2) buried pockmarks and 3) carbonates underlying or disconnected from the present-day
286 seafloor pockmarks.

287 Based on these observations and interpretations, the pockmarks along the Aquitaine
288 slope may have been formed by dewatering (Harrington, 1985), freshwater expulsion
289 (Whiticar, 2002) or short-duration gas escapes, associated with a relatively shallow source
290 level (the pockmarks being rooted a few metres to maximum a few tens of metres below the
291 seafloor) (Judd and Hovland, 1992). Indeed, gas releases over a long period of time (order of

kyears) would have led to authigenic carbonate precipitation (Andresen et al., 2008). Although the pockmarks along the Aquitaine slope are located away from the hydrate stability zone, it is unlikely with regards to the absence of fluid evidence that they were formed by gas hydrate dissociation as suspected along the U.S. Atlantic continental margin (Brothers et al., 2014). Moreover, the morphology and acoustic signature of the studied pockmarks do not fit those of hydrate-bearing pockmarks (Sultan et al., 2010). The latter are generally kilometre-large depressions with internal filling of disturbed sediments caused by hydrate destabilization. A few smaller pockmarks may be associated with these mega structures but exhibit disturbed sediments underneath (Davy et al., 2010).

Based on sub-bottom profiler data displayed in Gonthier et al. (2006) and in accordance with the seismic signature of pockmarks from our dataset, we suspected the occurrence of pockmarks within the recent sedimentary cover, which corresponds in the sediment wave field mainly to the so-called U4 unit (Faugères et al., 2002). This view is strengthened by the fact that above the pinch out of this unit U4 on the upper slope, roughly at water depth of 350 m, pockmarks are absent. This reinforces the shallow character (a few tens of metres maximum) of the Aquitaine slope pockmarks. The formation of the pockmarks appears therefore to postdate the sediment wave formation (U3 unit). Based on the age of the base of the 12-15 m thick U4 unit, which depends on the sediment rates, 10 cm/ky (Winnock, 1973) or 100 cm/ky (Schmidt et al., 2014, 2009), the pockmarks along the Aquitaine slope may have been initiated after 120-150 ky BP or 12-15 ky BP, respectively. Within this context, sea level falls may have triggered fluid escapes and initiation of pockmarks in the Aquitaine Basin as evidenced e. g. in the Gulf of Lions (Riboulot et al., 2014) and offshore West Africa (Plaza-Faverola et al., 2011). But without any detailed seismic data and dating of long cores through the Aquitaine slope, it is impossible to conclude.

316 With regards to the available data and the inactivity, morphology and repartition of the
317 studied Aquitaine pockmarks, there is no similarities with the other known, but not much
318 documented, fluid systems of the Bay of Biscay: 1) the Capbreton Canyon area where size-
319 differentiated pockmarks are related to different migration pathways (Baudon et al., 2013;
320 Gillet et al., 2008), 2) deeper offshore mega-pockforms on the Landes Plateau (Baudon et al.,
321 2013; Iglesias et al., 2010) and 3) gas emissions at the Aquitaine Shelf (Dupré et al., 2014a).

322 **5.2. Origin of pockmark elongation: slope, coalescence, currents?**

323 As it is assumed that pockmarks initially have a sub-circular shape (Judd and Hovland,
324 2007), why are the majority of the pockmarks (88%) located along the Aquitaine slope
325 (deeper than 350 m water depth) elongated ? With regards to inactivity and the absence of
326 present and past fluid evidence, it is unlikely that successive fluid releases have occurred, and
327 even less unlikely that this was able to reshape the pockmarks. The slope along which
328 pockmarks may become elongated and open downslope (Brothers et al., 2014) may be another
329 explanation for pockmark elongation. This may apply to some pockmarks in the sediment
330 wave field area but cannot account for all the depressions, as the directions of the slope and of
331 the elongated pockmarks are not compatible. Coalescence of several pockmarks may in places
332 explain some of the most elongated pockmarks observed along the Aquitaine slope, especially
333 in the northern part.

334 The influence of the bottom currents on pockmark morphology, namely their
335 elongation, has been evidenced across other continental shelves (Schattner et al., 2016) and
336 slopes (Tallobre et al., 2016), and is questioned here for the pockmarks along the Aquitaine
337 slope. Current-induced processes that can produce strong shear stress on the seafloor, such as
338 high density flow on the slope (Kuhnt et al., 2013) and internal tide impacting the seabed
339 (Pingree et al., 1986), may influence seafloor morphology. Along the Aquitaine slope, indirect
340 evidence of benthic material resuspension has been observed (Durrieu De Madron et al.,

341 1999; Kuhnt et al., 2013). The hypothesis put forward by Durrieu de Madron et al. (1999)
342 regarding the resuspension mechanism is an intensification of internal tidal current shear close
343 to the seabed, which happens to be tangent to the internal tide rays (Pingree et al., 1986) over
344 extensive areas of this region (Kuhnt et al., 2013). Direct observations of this process are still
345 lacking however, and it is thus hard to ascertain if this process is really dominant and if its
346 intensity is sufficient to have an impact on seafloor morphology along the Aquitaine slope.

347 The present-day bottom current direction does not correspond to the elongation
348 direction of the pockmarks along the Aquitaine slope. Two main current regimes are
349 evidenced, one driven by the semi-diurnal tide and mostly oriented east-west, and a second
350 long-period (period of a week) current mostly oriented north-south. In contrast, the pockmark
351 elongation varies in direction from NW-SE to WNW-ESE for the inter-canyon area and
352 sediment wave domain, respectively. Moreover, the 12% pockmarks which are sub-circular
353 occurring randomly amidst elongated ones are not coherent with the influence of a regional
354 bottom current.

355 Independently from the current direction, the velocities of the bottom currents, mainly
356 lower than 10 cm/s are not compatible with erosion. Current velocities of 10 cm/s are indeed
357 sufficient to limit sedimentation for silt and mud (Migniot, 1977) therefore preventing
358 pockmark filling. On the other hand, in order to remobilize consolidated silt, velocities higher
359 than 30 cm/s are necessary (Migniot, 1977). Thus, most of the present-day tide velocity and
360 N-S current velocity are not strong enough to remobilize sediment along the Aquitaine slope.
361 However, some stronger current events associated with higher velocities, such as the ones
362 observed reaching up to 34 cm/s in the along-slope S/N direction along the Aquitaine slope,
363 may contribute over short timescales to remobilize sediments within the pockmarks. Yet the
364 direction of these stronger bottom currents is not compatible with the direction of the
365 elongated pockmarks. Along the Aquitaine slope, these stronger events are clearly associated

366 with westerly-wind pulses occurring along the Cantabrian Slope (Batifoulier et al., 2012).
367 And the range of velocities recorded along the Aquitaine slope may induce regularly
368 upwelling within the depressions preventing fine sediments from being deposited (Brothers et
369 al., 2011; Hammer et al., 2009). This would not exclude the accumulation of coarser
370 sediments within the pockmark as inferred from the high seafloor backscatter of some of the
371 pockmarks.

372 Considering that circular pockmarks along the Aquitaine slope were formed at the
373 same time, the post-formation processes that have reshaped and elongated the pockmarks
374 along the WNW-ESE axis may be related to a former current regime that differs from the
375 present-day one. At present-day, upwelling induced by near-bottom currents within the
376 pockmarks may contribute to maintaining the depressions, preventing sedimentation by
377 winnowing out the fine grained sediments (Brothers et al., 2011; Hammer et al., 2009; Pau et
378 al., 2014). Relatively weak near-bottom currents along the U.S. Atlantic continental margin
379 (< 20 cm/s), as with those along the Aquitaine slope, appear sufficient to induce such
380 upwelling (Brothers et al., 2011). The few slightly elongated pockmarks (12%) corresponding
381 to subcircular pockmarks may be explained by subsequent filling-in possibly caused by
382 collapse within these former elongated pockmarks. It can be also considered that these
383 subcircular pockmarks may have been formed after the formation and subsequent elongation
384 by bottom currents of the initial majority of pockmarks.

385 **6. Conclusion**

386 The geophysical survey conducted on the Aquitaine slope revealed numerous
387 pockmarks (606) over 800 km² occurring on canyon interfluves and in the southern sediment
388 wave field from water depths of 350 m within the upper slope to greater depths westwards.
389 These pockmarks are relatively large, with the majority having a rough diameter between 100

390 and 200 m and an average internal depth of 15 m. Pockmarks along the Aquitaine slope are
391 divided into sub-circular (12%) and mostly elongated (88%) pockmarks including some
392 coalescent. The slope and the coalescence of pockmarks, as the primary controlling factor,
393 only constrains the elongation of part of the pockmarks. But the majority of elongated
394 pockmarks are not aligned along the present-day prevailing current direction as it is the case
395 across other continental shelves and slopes (Bøe et al., 1998; Schattner et al., 2016; Tallobre
396 et al., 2016). Pockmarks along the Aquitaine slope are not randomly distributed with regards
397 to the water depth and surrounding morphology. Slope-indenting submarine canyons are
398 pockmark free zones as observed along e. g. shelf-indenting canyons (Brothers et al., 2014).
399 In the north of the studied area, pockmarks are constrained by the E-W oriented inter-canyon
400 morphology while in the southern area, they are generally oriented NNE-SSW along the
401 direction of the crests and inter-crests from the sediment wave system. There is no positive
402 correlation between the dimension of the pockmark and water depths as has been observed
403 elsewhere (Gafeira et al., 2012; Schattner et al., 2016). Instead, pockmark size appears more
404 often influenced by the nature and thickness of sediments (Baltzer et al., 2014; King and
405 MacLean, 1970; Rise et al., 2015) than the water depth. Along the Aquitaine continental
406 slope, the thickness of the upper most sedimentary layer, the unit U4 as defined by Faugères
407 et al. (2002) and Gonthier et al (2006), appears indeed to drive the occurrence of pockmarks.
408 Thus, the pockmark distribution is sedimentologically controlled by 1) the presence and the
409 thickness of the uppermost sedimentary cover, which is a few metres to a few tens of metres
410 thick, with 2) a secondary influence of inherited sedimentary structures such as the sediment
411 waves.

412 The history of the Aquitaine slope pockmarks is recent with regards to the Aquitaine
413 margin history and can be described as three main stages. Fluid migration from a shallow
414 source level, a few metres to a few tens of metres below the present-day seafloor, and fluid

415 expulsion at the seabed have led to the formation of circular pockmarks. These pockmarks
416 were initiated not before the Holocene times, and possibly within the last 10 kyears. These
417 pockmarks were most likely formed by past short-duration fluid-release events associated
418 with microbial gas (methane) or possibly water without major associated diagenesis, as
419 methane-derived authigenic carbonate precipitation. Then, near-bottom currents, different in
420 orientation and velocity than present-day ones, have modified the pockmarks from circular to
421 elongated ones in the WNW-ESE direction. This was possibly followed by a second but
422 minor formation of pockmarks unless the 12% of subcircular pockmarks are former elongated
423 ones that were modified later on by sediment infilling or collapse. At present-day, the
424 Aquitaine slope is dominated by weaker near-bottom currents which may induce upwelling
425 within the inactive pockmarks, contributing to the maintenance of their shape as proposed,
426 observed and modelled for other studied cases (Brothers et al., 2011; Hammer et al., 2009;
427 Pau et al., 2014).

428 **Acknowledgments**

429 The GAZCOGNE study, the marine expedition GAZCOGNE1
430 (<http://dx.doi.org/10.17600/13020070>) and the PhD thesis of Guillaume Michel were co-
431 funded by TOTAL and IFREMER as part of the PAMELA (<http://dx.doi.org/10.18142/236>)
432 (Passive Margin Exploration Laboratories) scientific project. The BOBGEO2
433 (<http://dx.doi.org/10.17600/10020020>) marine expedition was part of the FP7 EU Project
434 CORALFISH. The ASPEX2010A survey (<http://dx.doi.org/10.17600/10020010>) was part of
435 the EPIGRAM project. The authors wish to thank Johan Saout, Charline Guerin, Cécile
436 Breton, Emeric Gautier, Elodie Petit, Romain Biville and André Ogor for their contribution to
437 data processing, Joana Gafeira for her discussions on pockmark detection, Alison Chalm and

438 Ewan Harney for English correction and the two reviewers, Hervé Gillet and Soledad Garcia-
439 Gil for their helpful comments.

440

Accepted version CRG

442 **References**

- 443 Andresen, K.J., Huuse, M., Clausen, O.R., 2008. Morphology and distribution of Oligocene
444 and Miocene pockmarks in the Danish North Sea-implications for bottom current activity
445 and fluid migration. *Basin Res.* 20, 445–466. doi:10.1111/j.1365-2117.2008.00362.x
- 446 Baltzer, A., Ehrhold, A., Rigolet, C., Souron, A., Cordier, C., Clouet, H., Dubois, S.F., 2014.
447 Geophysical exploration of an active pockmark field in the Bay of Concarneau, southern
448 Brittany, and implications for resident suspension feeders. *Geo-Marine Lett.* 34, 215–
449 230. doi:10.1007/s00367-014-0368-0
- 450 Batifoulier, F., Lazure, P., Bonneton, P., 2012. Poleward coastal jets induced by westerlies in
451 the Bay of Biscay. *J. Geophys. Res. Ocean.* 117, 1–19. doi:10.1029/2011JC007658
- 452 Baudon, C., Gillet, H., Cremer, M., 2013. Focused fluid-flow processes through high-quality
453 bathymetric, 2D seismic and Chirp data from the southern parts of the Bay of Biscay,
454 France, in: EGU General Assembly Conference Abstracts. pp. 763.
- 455 Bayon, G., Loncke, L., Dupré, S., Caprais, J.C., Ducassou, E., Duperron, S., Etoubleau, J.,
456 Foucher, J.P., Fouquet, Y., Gontharet, S., Henderson, G.M., Huguen, C., Klaucke, I.,
457 Mascle, J., Migeon, S., Olu-Le Roy, K., Ondréas, H., Pierre, C., Sibuet, M., Stadnitskaia,
458 A., Woodside, J., 2009. Multi-disciplinary investigation of fluid seepage on an unstable
459 margin: The case of the Central Nile deep sea fan. *Mar. Geol.* 261, 92–104.
460 doi:10.1016/j.margeo.2008.10.008
- 461 Biteau, J.-J., Le Marrec, A., Le Vot, M., Masset, J.-M., 2006. The Aquitaine Basin. *Pet.*
462 *Geosci.* 12, 247–273. doi:10.1144/1354-079305-674
- 463 Bøe, R., Rise, L., Ottesen, D., 1998. Elongate depressions on the southern slope of the
464 Norwegian Trench (Skagerrak): Morphology and evolution. *Mar. Geol.* 146, 191–203.
465 doi:10.1016/S0025-3227(97)00133-3
- 466 Brothers, D.S., Ruppel, C., Kluesner, J.W., Ten Brink, U.S., Chaytor, J.D., Hill, J.C.,
467 Andrews, B.D., Flores, C., 2014. Seabed fluid expulsion along the upper slope and outer
468 shelf of the U.S. Atlantic continental margin. *Geophys. Res. Lett.* 41, 96–101.
469 doi:10.1002/2013GL058048
- 470 Brothers, L.L., Kelley, J.T., Belknap, D.F., Barnhardt, W.A., Andrews, B.D., Maynard, M.L.,
471 2011. More than a century of bathymetric observations and present-day shallow
472 sediment characterization in Belfast Bay, Maine, USA: Implications for pockmark field
473 longevity. *Geo-Marine Lett.* 31, 237–248. doi:10.1007/s00367-011-0228-0
- 474 Charria, G., Lazure, P., Le Cann, B., Serpette, A., Reverdin, G., Louazel, S., Batifoulier, F.,
475 Dumas, F., Pichon, A., Morel, Y., 2013. Surface layer circulation derived from
476 Lagrangian drifters in the Bay of Biscay. *J. Mar. Syst.* 109, S60–S76.
477 doi:10.1016/j.jmarsys.2011.09.015
- 478 Cirac, P., Berne, S., Castaing, P., Weber, O., 2000. Processus de mise en place et d'évolution
479 de la couverture sédimentaire superficielle de la plate-forme nord-aquitaine. *Oceanol.*
480 *Acta* 23, 663–686.
- 481 Dandapath, S., Chakraborty, B., Karisiddaiah, S.M., Menezes, A., Ranade, G., Fernandes, W.,
482 Naik, D.K., Prudhvi Raju, K.N., 2010. Morphology of pockmarks along the western
483 continental margin of India: Employing multibeam bathymetry and backscatter data.
484 *Mar. Pet. Geol.* 27, 2107–2117. doi:10.1016/j.marpetgeo.2010.09.005
- 485 Davy, B., Pecher, I., Wood, R., Carter, L., Gohl, K., 2010. Gas escape features off New

486 Zealand: Evidence of massive release of methane from hydrates. *Geophys. Res. Lett.* 37,
487 1–5. doi:10.1029/2010GL045184

488 Dupré, S., Berger, L., Le Bouffant, N., Scalabrin, C., Bourillet, J.F., 2014a. Fluid emissions at
489 the Aquitaine Shelf (Bay of Biscay, France): A biogenic origin or the expression of
490 hydrocarbon leakage? *Cont. Shelf Res.* 88, 24–33. doi:10.1016/j.csr.2014.07.004

491 Dupré, S., Mascle, J., Foucher, J.P., Harmegnies, F., Woodside, J., Pierre, C., 2014b. Warm
492 brine lakes in craters of active mud volcanoes, Menes caldera off NW Egypt: Evidence
493 for deep-rooted thermogenic processes. *Geo-Marine Lett.* 34, 153–168.
494 doi:10.1007/s00367-014-0367-1

495 Dupré, S., Scalabrin, C., Grall, C., Augustin, J.-M., Henry, P., Sengör, A.M., Görür, N.,
496 Çagatay, M.N., Géli, L., 2015. Tectonic and sedimentary controls on widespread gas
497 emissions in the Sea of Marmara: Results from systematic, shipborne multibeam echo
498 sounder water column imaging. *J. Geophys. Res. Solid Earth* 120, 2891–2912.

499 Dupré, S., Woodside, J., Klauke, I., Mascle, J., Foucher, J.P., 2010. Widespread active
500 seepage activity on the Nile Deep Sea Fan (offshore Egypt) revealed by high-definition
501 geophysical imagery. *Mar. Geol.* 275, 1–19. doi:10.1016/j.margeo.2010.04.003

502 Durrieu De Madron, X., Castaing, P., Nyffeler, F., Courp, T., 1999. Slope transport of
503 suspended particulate matter on the Aquitanian margin of the Bay of Biscay. *Deep. Res.*
504 *Part II Top. Stud. Oceanogr.* 46, 2003–2027. doi:10.1016/S0967-0645(99)00053-3

505 Faugères, J.-C., Gonthier, E., Mulder, T., Kenyon, N., Cirac, P., Gribouard, R., Berné, S.,
506 Lesuavé, R., 2002. Multi-process generated sediment waves on the Landes Plateau (Bay
507 of Biscay, North Atlantic). *Mar. Geol.* 182, 279–302. doi:10.1016/S0025-
508 3227(01)00242-0

509 Gafeira, J., Long, D., Diaz-Doce, D., 2012. Semi-automated characterisation of seabed
510 pockmarks in the central North Sea. *Near Surf. Geophys.* 10, 303–315.
511 doi:10.3997/1873-0604.2012018

512 Gay, A., Lopez, M., Berndt, C., Séranne, M., 2007. Geological controls on focused fluid flow
513 associated with seafloor seeps in the Lower Congo Basin. *Mar. Geol.* 244, 68–92.
514 doi:10.1016/j.margeo.2007.06.003

515 Gay, A., Lopez, M., Ondreas, H., Charlou, J.L., Sermondadaz, G., Cochonat, P., 2006.
516 Seafloor facies related to upward methane flux within a Giant Pockmark of the Lower
517 Congo Basin. *Mar. Geol.* 226, 81–95. doi:10.1016/j.margeo.2005.09.011

518 Gillet, H., Cirac, P., Lagié, B., 2008. Pockmarks on the southern margin of the Capbreton
519 Canyon (south-eastern Bay of Biscay), in: Borja, A. (Ed.), XI International Symposium
520 on Oceanography of the Bay of Biscay. “Revisa de Investgacion Marina” 3, San
521 Sebastian, pp. 90–91.

522 Gonthier, E., Cirac, P., Faugères, J.C., Gaudin, M., Cremer, M., Bourillet, J.F., 2006.
523 Instabilities and deformation in the sedimentary cover on the upper slope of the southern
524 Aquitaine continental margin, north of the Capbreton canyon (Bay of Biscay). *Sci. Mar.*
525 70, 89–100. doi:10.3989/scimar.2006.70s189

526 Hammer, Ø., Webb, K.E., Depreiter, D., 2009. Numerical simulation of upwelling currents in
527 pockmarks, and data from the Inner Oslofjord, Norway. *Geo-Marine Lett.* 29, 269–275.
528 doi:10.1007/s00367-009-0140-z

529 Harrington, P.K., 1985. Formation of pockmarks by pore-water escape. *Geo-Marine Lett.* 5,
530 193–197.

531 Hovland, M., Heggland, R., De Vries, M.H., Tjelta, T.I., 2010. Unit-pockmarks and their
532 potential significance for predicting fluid flow. *Mar. Pet. Geol.* 27, 1190–1199.
533 doi:10.1016/j.marpetgeo.2010.02.005

534 Iglesias, J., Ercilla, G., García-Gil, S., Judd, A.G., 2010. Pockforms: An evaluation of
535 pockmark-like seabed features on the Landes Plateau, Bay of Biscay. *Geo-Marine Lett.*

536 30, 207–219. doi:10.1007/s00367-009-0182-2

537 Josenhans, H.W., King, L.H., Fader, G.B., 1978. A side-scan sonar mosaic of pockmarks on
538 the Scotian Shelf. *Can. J. Earth Sci.* 15, 831–840.

539 Judd, A., Hovland, M., 2007. *Seabed fluid flow: the impact on geology, biology and the*
540 *marine environment.* Cambridge University Press, p. 239.

541 Judd, A.G., Hovland, M., 1992. The evidence of shallow gas in marine sediments. *Cont. Shelf*
542 *Res.* 12, 1081–1095. doi:10.1016/0278-4343(92)90070-Z

543 Kersalé, M., Marie, L., Le Cann, B., Serpette, A., Lathuilière, C., Le Boyer, A., Rubio, A.,
544 Lazure, P., 2016. Poleward along-shore current pulses on the inner shelf of the Bay of
545 Biscay. *Estuar. Coast. Shelf Sci.* 179, 155–171.

546 King, L.H., MacLean, B., 1970. Pockmarks on the Scotian Shelf. *Bull. Geol. Soc. Am.* 81,
547 3141–3148. doi:10.1130/0016-7606(1970)81[3141:POTSS]2.0.CO;2

548 Kuhnt, T., Howa, H., Schmidt, S., Marié, L., Schiebel, R., 2013. Flux dynamics of planktic
549 foraminiferal tests in the south-eastern Bay of Biscay (northeast Atlantic margin). *J. Mar.*
550 *Syst.* 109, 169–181.

551 Lazure, P., Garnier, V., Dumas, F., Herry, C., Chifflet, M., 2009. Development of a
552 hydrodynamic model of the Bay of Biscay. Validation of hydrology. *Cont. Shelf Res.* 29,
553 985–997.

554 Le Boyer, A., Charria, G., Le Cann, B., Lazure, P., Marié, L., 2013. Circulation on the shelf
555 and the upper slope of the Bay of Biscay. *Cont. Shelf Res.* 55, 97–107.
556 doi:10.1016/j.csr.2013.01.006

557 Michel, G., Dupré, S., Saout, J., Ehrhold, A., Guerin, C., Gautier, E., Breton, C., Bourillet, J.-
558 F., Loubrieu, B., 2017. Pockmark morphological attributes at the Aquitaine slope,
559 GAZCOGNE1 (2013) and BOBGEO2 (2010) marine expeditions. SEANOE Database
560 <http://doi.org/10.17882/48323>. doi:10.17882/48323

561 Migniot, C., 1977. Action des courants, de la houle et du vent sur les sédiments. *La Houille*
562 *Blanche* 1, 9–47.

563 Moss, J.L., Cartwright, J., Moore, R., 2012. Evidence for fluid migration following pockmark
564 formation: Examples from the Nile Deep Sea Fan. *Mar. Geol.* 303, 1–13.
565 doi:10.1016/j.margeo.2012.01.010

566 Pau, M., Gisler, G., Hammer, Ø., 2014. Experimental investigation of the hydrodynamics in
567 pockmarks using particle tracking velocimetry. *Geo-Marine Lett.* 34, 11–19.
568 doi:10.1007/s00367-013-0348-9

569 Pau, M., Hammer, Ø., 2013. Sediment mapping and long-term monitoring of currents and
570 sediment fluxes in pockmarks in the Oslofjord, Norway. *Mar. Geol.* 346, 262–273.
571 doi:10.1016/j.margeo.2013.09.012

572 Pilcher, R., Argent, J., 2007. Mega-pockmarks and linear pockmark trains on the West
573 African continental margin. *Mar. Geol.* 244, 15–32. doi:10.1016/j.margeo.2007.05.002

574 Pingree, R.D., Mardell, G.T., New, A.L., 1986. Propagation of internal tides from the upper
575 slopes of the Bay of Biscay. *Nature* 321, 154–158. doi:10.1038/321154a0

576 Plaza-Faverola, A., Bünz, S., Mienert, J., 2011. Repeated fluid expulsion through sub-seabed
577 chimneys offshore Norway in response to glacial cycles. *Earth Planet. Sci. Lett.* 305,
578 297–308.

579 Riboulot, V., Thomas, Y., Berné, S., Jouet, G., Cattaneo, A., 2014. Control of Quaternary sea-
580 level changes on gas seeps. *Geophys. Res. Lett.* 41, 4970–4977.

581 Rise, L., Bellec, V.K., Chand, S., Bøe, R., 2015. Pockmarks in the southwestern Barents Sea
582 and - Finnmark fjords. *Nor. J. Geol.* 94, 263–282.

583 Roca, E., Muñoz, J.A., Ferrer, O., Ellouz, N., 2011. The role of the Bay of Biscay Mesozoic
584 extensional structure in the configuration of the Pyrenean orogen: Constraints from the
585 MARCONI deep seismic reflection survey. *Tectonics* 30, 1–33.

586 doi:10.1029/2010TC002735
587 Schattner, U., Lazar, M., Souza, L.A.P., Ten Brink, U., Mahiques, M.M., 2016. Pockmark
588 asymmetry and seafloor currents in the Santos Basin offshore Brazil. *Geo-Marine Lett.*
589 36, 457–464. doi:10.1007/s00367-016-0468-0
590 Schmidt, S., Howa, H., Diallo, A., Martin, J., Cremer, M., Duros, P., Fontanier, C., Deflandre,
591 B., Metzger, E., Mulder, T., 2014. Recent sediment transport and deposition in the Cap-
592 Ferret Canyon, South-East margin of Bay of Biscay. *Deep Sea Res. Part II Top. Stud.*
593 *Oceanogr.* 104, 134–144.
594 Schmidt, S., Howa, H., Mouret, A., Lombard, F., Anschutz, P., Labeyrie, L., 2009. Particle
595 fluxes and recent sediment accumulation on the Aquitanian margin of Bay of Biscay.
596 *Cont. Shelf Res.* 29, 1044–1052.
597 Sibuet, J.C., Monti, S., Loubrieu, B., Mazé, J.-P., Srivastava, S., 2004. Carte bathymétrique
598 de l'Atlantique nord-est et du golfe de Gascogne : implications cinématiques. *Bull. la*
599 *Soc. Geol. Fr.* Tome 175, 429–442.
600 Sultan, N., Marsset, B., Ker, S., Marsset, T., Voisset, M., Vernant, A.-M., Bayon, G., Cauquil,
601 E., Adamy, J., Colliat, J.L., others, 2010. Hydrate dissolution as a potential mechanism
602 for pockmark formation in the Niger delta. *J. Geophys. Res. Solid Earth* 115, 33.
603 Tallobre, C., Loncke, L., Bassetti, M.A., Giresse, P., Bayon, G., Buscail, R., de Madron,
604 X.D., Bourrin, F., Vanhaesebroucke, M., Sotin, C., 2016. Description of a contourite
605 depositional system on the Demerara Plateau: Results from geophysical data and
606 sediment cores. *Mar. Geol.* 378, 56–73. doi:10.1016/j.margeo.2016.01.003
607 Van Aken, H.M., 2000. The hydrography of the mid-latitude Northeast Atlantic Ocean II: The
608 intermediate water masses. *Deep. Res. Part I Oceanogr. Res. Pap.* 47, 789–824.
609 doi:10.1016/S0967-0637(99)00112-0
610 Webb, K.E., Hammer, Ø., Lepland, A., Gray, J.S., 2009. Pockmarks in the inner Oslofjord,
611 Norway. *Geo-Marine Lett.* 29, 111–124.
612 Whiticar, M.J., 2002. Diagenetic relationships of methanogenesis, nutrients, acoustic
613 turbidity, pockmarks and freshwater seepages in Eckernförde Bay. *Mar. Geol.* 182, 29–
614 53.
615 Winnock, E., 1973. Exposé succinct de l'évolution paleogeologique de l'Aquitaine. *Bull. la*
616 *Soc. Geol. Fr.* 7, 5–12.
617
618

619 **Figure captions**

620

621 Fig. 1: Synthetic map of the Bay of Biscay with indication of the main current regimes (see references
622 therein) and main isobaths (Sibuet et al., 2004). The study area (red rectangle) covers the western
623 extension of the Parentis Basin (Biteau et al., 2006) and the eastern Landes Plateau.

624

625 Fig. 2: a) Detailed shaded bathymetry map of the Aquitaine Margin with main seafloor morphologies:
626 pockmarks, canyons and sediment waves. Background bathymetry from EMODnet Bathymetry portal
627 (<http://www.emodnet-bathymetry.eu>). ASPEX current mooring 10 is located at a water depth of 450 m
628 in the sediment wave field. Slope focus on b) elongated pockmarks in the northern inter-canyon area
629 and c) sub-circular pockmarks in the sediment wave field.

630

631 Fig. 3: Processed sub-bottom profiler line displayed in envelope in ©Kingdom Software. X axis
632 corresponds to Shot Point (SP) and Y axis to depth in seconds in Two Way Time (TWT). The profile
633 is displayed with a Vertical Exaggeration (VE) of 7, calculated with a seismic wave velocity of 1500
634 m/s, with indication of slope angle. This sub-bottom profiler line crosses two pockmarks (see location
635 in Fig. 2a) without any fluid evidence and exhibits only triplication points, so-called "bow tie"
636 artefacts.

637

638 Fig. 4: Box plots of a) pockmark area with indication of diameter with regards to pockmark surface (a
639 circular pockmark with a diameter of 200 m corresponds to a surface of $3 \times 10^4 \text{ m}^2$), b) pockmark
640 seafloor backscatter amplitude from the 30 kHz EM302 multibeam data and c) pockmark elongation.
641 Red curves in maps stand for the contour of pockmarks. The legend of the box plots is displayed in
642 Fig. 4c, with representation of the minimum, maximum, first quartile (Q25), second quartile (Q50 or
643 median), third quartile (Q75) of the series and series outliers.

644 Fig. 5: Rose diagrams of the pockmark major axis direction and local slope direction around
645 pockmarks for a) inter-canyon and b) sediment wave areas. Arrow and shape lengths are proportional
646 to the number of pockmarks involved. Recorded velocity and orientation of currents from ASPEX
647 mooring 10 are shown in black and red dots for raw and tide-filtered data, respectively. c) Diagram of
648 spatial distribution of current velocities and orientations of raw signals.
649

Accepted version CRG

650

651 **Supplementary Material**

652 **Appendix A. Morphometric methods**

653 Three methods to map pockmarks were tested, two semi-automated and one manual to check
654 the validity of the two previous. The Fill method (Gafeira et al., 2012) involves pockmark
655 extraction based on a succession of Geographical Information System (GIS) operations
656 focused on the numerical filling of depressions and then the subtraction of filled bathymetry.
657 The second method called the BPI (Bathymetric Position Index, Wright et al., 2012) is based
658 on the calculation of differential bathymetry cells side by side and seafloor roughness
659 analysis. Both semi-automated methods map a large number of depressions which are not
660 pockmarks. Around 500 times more features than manually mapped pockmarks were detected
661 with the Fill method and 300 times more with the BPI method. For both semi-automated
662 methods, the detected features were filtered with correction based on the pockmark surface
663 and the surface/perimeter ratio. Features with small ratio are more likely to be an artefact
664 (Gafeira et al., 2012). The number of remaining features is 10 and 20 times higher than the
665 number of manually mapped pockmarks, with Fill and BPI methods respectively and most
666 likely corresponds to spurious pockmarks and artefacts which have not been filtered.
667 Therefore, in order to minimize the biases observed with semi-automatic methods, all
668 pockmarks were manually delimited.

669 Pockmark internal depths were calculated in two ways, using the Fill method
670 developed in Gafeira et al. (2012) and by calculating the difference between the maximum
671 and minimum bathymetric values over the delimited pockmark surface. The calculation of
672 pockmark internal depth based on the method by Gafeira et al. (2012) leads to strongly
673 minimize the internal depth of the studied pockmarks with results showing that most of the

674 pockmarks (82%) have an internal depth <1 m and 8% have an internal depth of 0 m. Instead,
675 the method based on the difference between maximum and minimum bathymetry provides
676 realistic values. It is clear from our results that the Fill method is not able to calculate the
677 effective infilling of the studied pockmarks, most likely because of their irregular morphology
678 (e. g. collapsed flank) and regional slope of 3°. Thus, this method suits uniform areas with
679 well-shaped pockmarks (Gafeira et al., 2012; Geldof et al., 2014) but does not fit with
680 complex morphologies with slopes. In the latter case, it is more appropriate to calculate the
681 internal depth by subtracting the maximum bathymetry over the entire pockmark from the
682 minimum one.

683 Both semi-automatic methods and manual picking show advantages and drawbacks.
684 Semi-automatic methods are based on a succession of quick numerical calculations, but most
685 of these latter have to be manually checked to limit the number of artefacts. 5433 features
686 were detected as depressions with the “Fill” method (Gafeira et al., 2012) and 10437 with the
687 BPI method (Wright et al., 2012) whereas the manual picking only gives 606 pockmarks. The
688 elimination of a large amount of artefacts is time-consuming, hence defeating one of the main
689 advantages of semi-automatic methods. Although manual picking is considered time-
690 consuming, it is much more appropriate in the case of complex seafloor morphologies due to
691 the human capability to focus on features of interest. Indeed, along the Aquitaine slope, there
692 is the superimposition of different scale morphologies such as slope, canyons and sediment
693 waves that prevent the semi-automated detection process from being accurate. Thus, semi-
694 automatic methods should be used in relatively flat bathymetry areas to obtain successful
695 results, e. g. at continental shelves (Gafeira et al., 2012), bays (Andrews et al., 2010) and in
696 basins (Geldof et al., 2014). For large extents and huge densities but of similar features, the
697 automatic methods are clearly efficient (Andrew et al., 2010; Gafeira et al., 2012; Geldof et
698 al., 2014). Semi-automatic methods to map pockmarks are not appropriate in the study area

699 because of the complex bathymetry inherited from several orders of morphologies, the slope
700 angle and the presence of features such as canyons and sediment waves. Pockmark
701 morphometry was therefore based on manual mapping.

702 Andrews, B.D., Brothers, L.L., Barnhardt, W.A., 2010. Automated feature extraction and
703 spatial organization of seafloor pockmarks, Belfast Bay, Maine, USA. *Geomorphology*
704 124, 55–64. doi:10.1016/j.geomorph.2010.08.009

705 Geldof, J., Gafeira, J., Contet, J., Marquet, S., 2014. GIS Analysis Of Pockmarks From 3D
706 Seismic Exploration Surveys, in: *Offshore Technology Conference*. Houston USA,
707 OTC 25088.

708 Wright, D.J., Pendleton, M., Boulware, J., Walbridge, S., Gerlt, B., Eslinger, D., Sampson,
709 D., Huntley, E., 2012. ArcGIS Benthic Terrain Modeler (BTM), v. 3.0, Environmental
710 Systems Research Institute, NOAA Coastal Services Center, Massachusetts Office of
711 Coastal Zone Management [WWW Document]. ESRI. URL
712 <https://www.arcgis.com/home/item.html?id=b0d0be66fd33440d97e8c83d220e7926>

713 **Appendix B.**

714 Figure including scatter plots of pockmark surface versus bathymetry with internal depth as point
715 colour, for both a) inter-canyon and b) sediment wave areas with regression lines and determination
716 coefficients (R^2).

717 **Appendix C.**

718 Figure exhibiting bottom current velocity, a) east-west (U_E) and b) north-south (U_N) components,
719 recorded with ASPEX mooring 10 (see location in Fig. 2). Current velocities are integrated between
720 17 m and 33 m above the seafloor. Recorded velocity and orientation of currents are shown in blue
721 and red curves for raw and tide-filtered data, respectively.

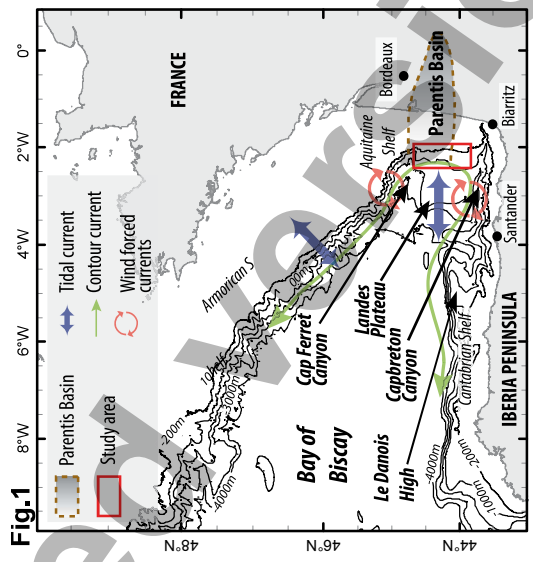
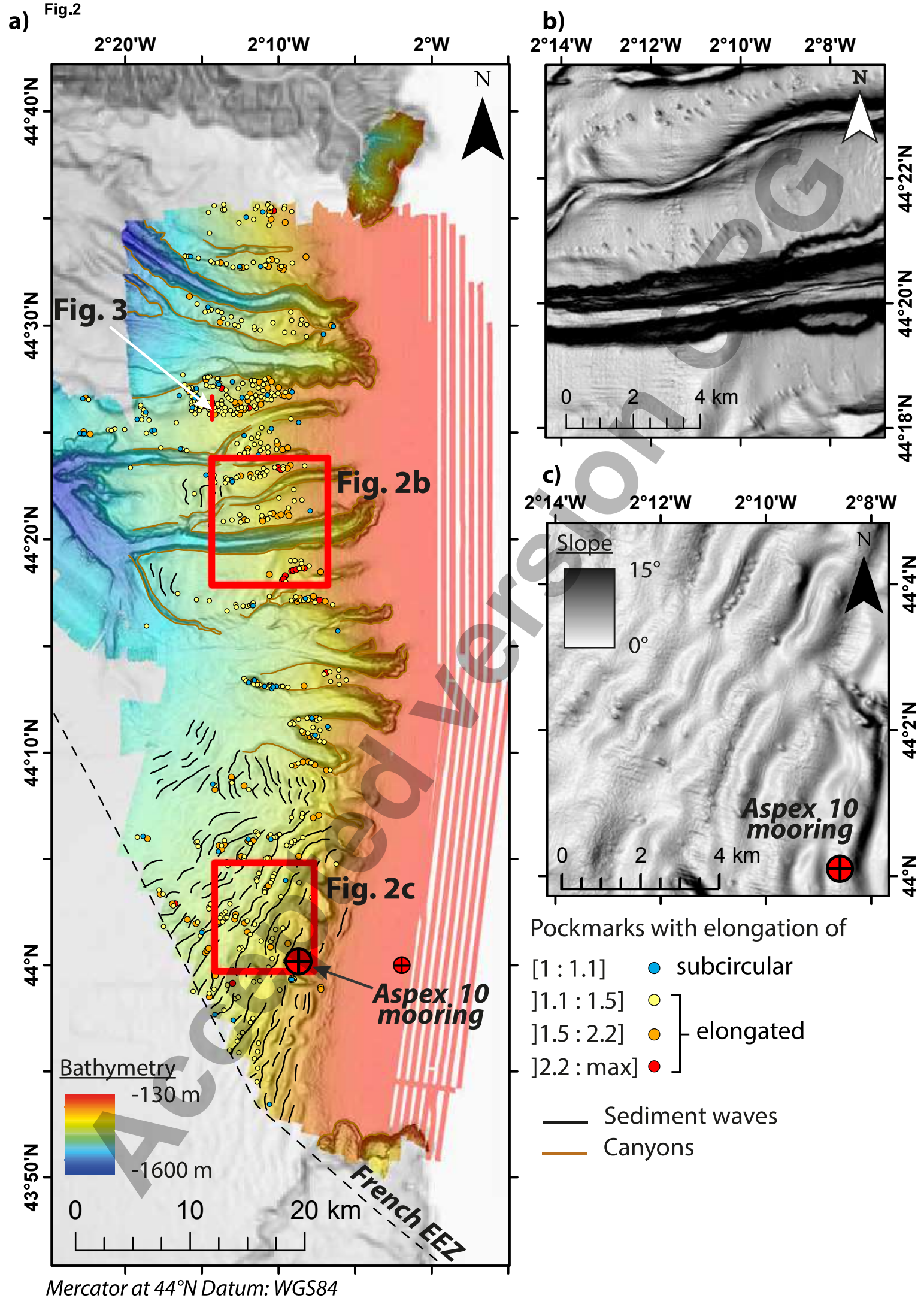


Fig.1



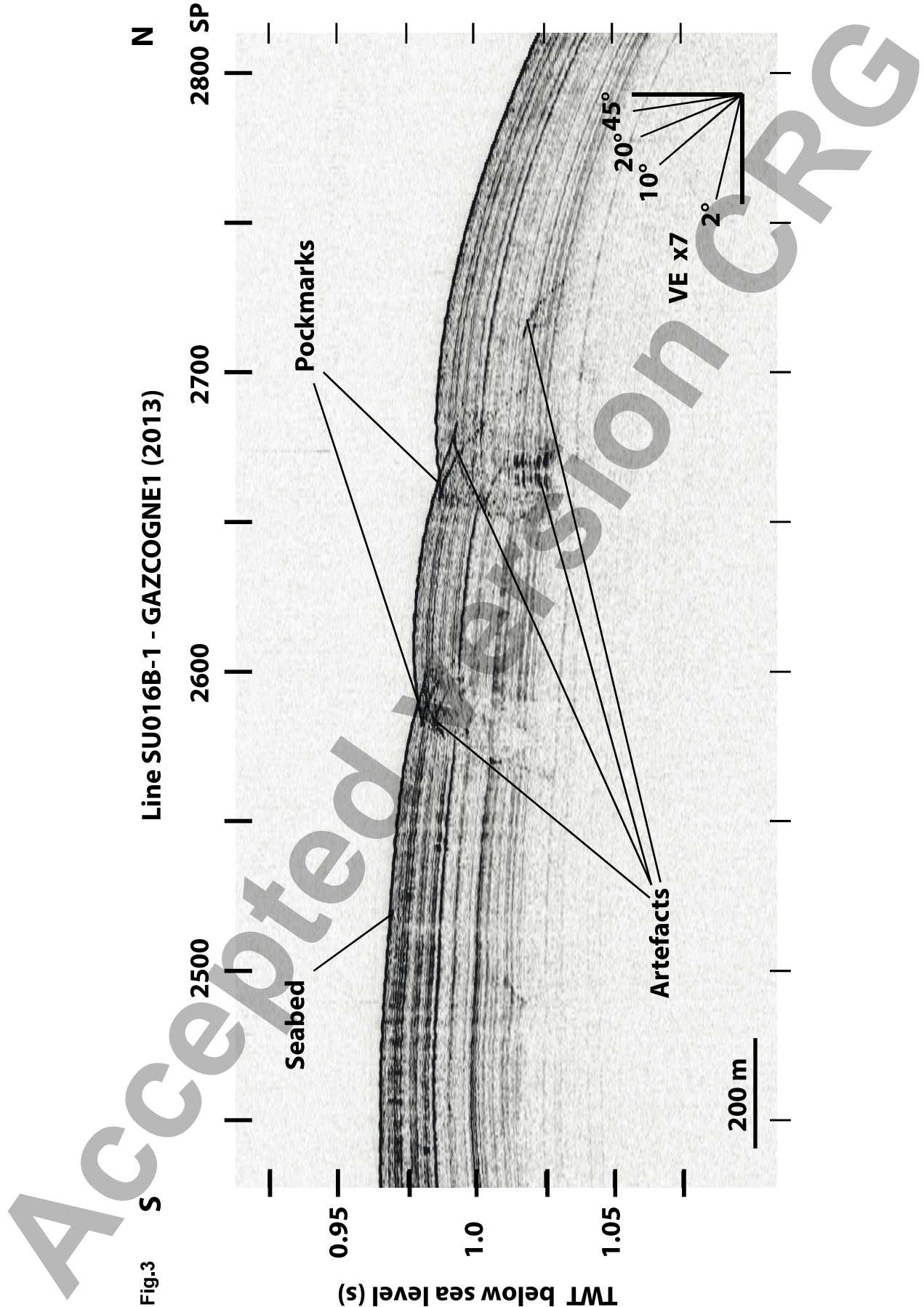


Fig.3 S Line SU016B-1 - GAZCOGNE1 (2013) N

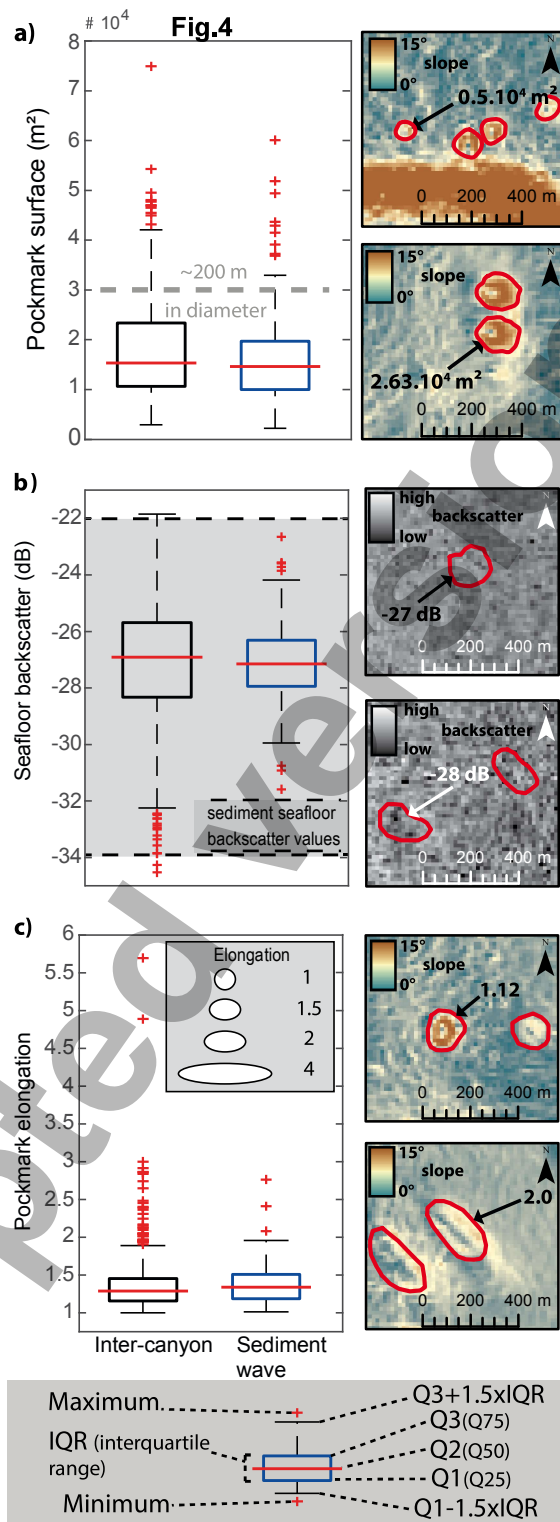
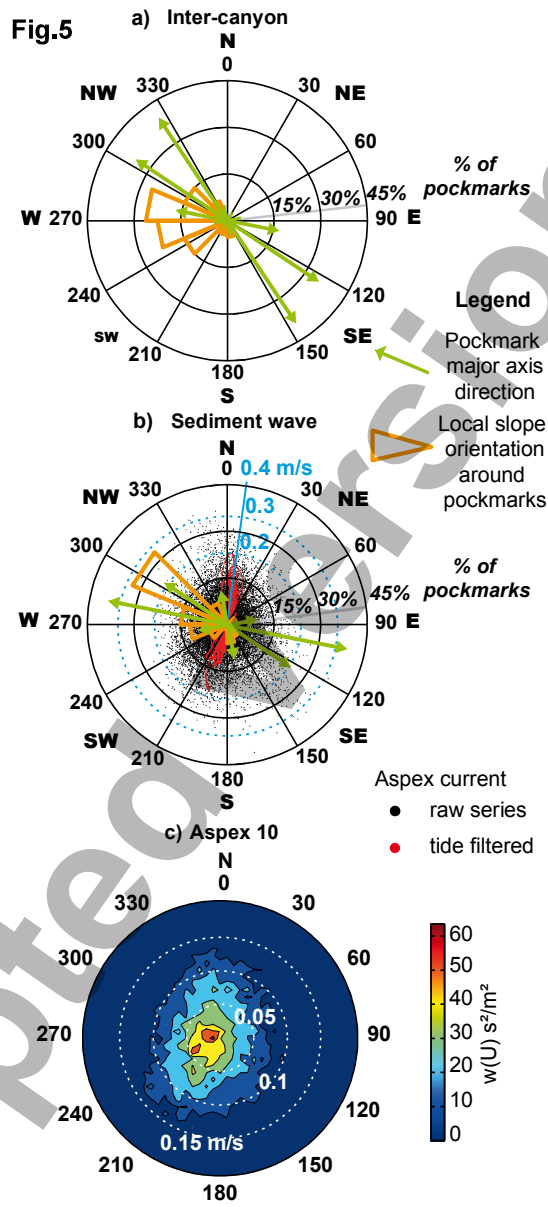
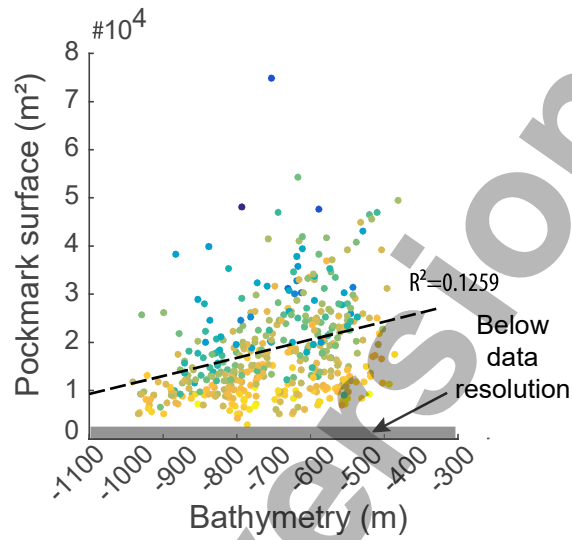


Fig.5



a) Inter-canyon Appendix B



b) Sediment wave

